International Journal of Innovative
Computing, Information and Control
Volume **15**, Number **2**, April **2019**

ICIC International ©2019 ISSN 1349-4198
pp. **489–501**

ADAPTIVE LOOK-UP TABLE AND INTERPOLATED PI GAIN SCHEDULING CONTROL FOR VOLTAGE REGULATOR USING DC-DC CONVERTER

Faizal Arya Samman[1,*], Channareth Srun[2] and Rhiza Samsoe'oed Sadjad[1]

[1]Department of Electrical Engineering
Universitas Hasanuddin
Kampus Gowa, Jl. Poros Malino Km. 6, Bontomarannu 92171, South Sulawesi, Indonesia
[*]Corresponding author: faizalas@unhas.ac.id

[2]Department of Electronic Engineering
National Polytechnic Institute of Cambodia
Phum Prey Popel, SK. Somrong Krom, Khan Po Sen Chey, Phnom Penh 12000, Cambodia

Received May 2018; revised October 2018

Abstract. *This paper presents semi-adaptive proportional-integral (PI) gain scheduling methods used to control the 220V direct current (DC) output voltage of a DC-DC converter. The constant output voltage is useful for the input voltage of an AC-DC inverter utilized in a micro-scale photovoltaic (PV) power systems, also for DC integration with a rectified existing AC grid. The PI control gains are scheduled based on two approaches, namely interpolated and look-up table methods. The control gains are obtained from offline explorations of the best PI gains for some load conditions and input voltage domains, where maximum peak overshoot and average absolute voltage error are used as the criteria to select them. These selected gains are then used to construct an interpolation function and a look-up table. During runtime control process, the PI gains are then scheduled or selected from the interpolation function or from the look-up table. The performance of the proposed control methods has been compared with the traditional static PI control. The results present that the adaptive look-up table (LUT) PI gain scheduling control method gives the best performance over the static and adaptive interpolated PI gain scheduling methods. Measured relative over the expected 220V, its average absolute output voltage error is below 1.141% with maximum overshoot about 5.6%.*

Keywords: Power electronics, Voltage regulator, PI gain scheduling control, Semi-adaptive control, DC-DC converter

1. **Introduction.** Fossil fuels have long time become important energy sources for industries and human activities. However, environmental issues and the reduction of fossil fuel resources in earth are the main points that challenge many researches to find new, renewable and sustainable alternative energy resources. Not similar to steam-engine generator powered by fossil fuels, renewable energy converters generate unpredictable electric power, because most of renewable energies are ambient energy sources. Due to the problem, the integration of the renewable-energy-based power generations with fossil fuel electric power generations in large scale power systems is a crucial problem, especially to balance power demand and power generation in a most economical operational point. Relatively low power capacity and power efficiency are other challenging issues. Those issues have been investigated by many researchers to improve them. New inventions and innovations in this research field will change the way we electrify our daily life.

DOI: 10.24507/ijicic.15.02.489

There are many renewable energy sources such as solar energy, wind, and tidal energy. Solar energy, which is converted by photovoltaic (PV) cells to be electric energy, is a primary energy source. Therefore, its utilization in future electric power systems will be very important. Another challenging problem, which is discussed in this paper, is the integration of the AC power source from 220V/230V-grid with the PV modules, in home-scale or micro-grid-scale power systems. In AC coupling or integration, frequency, amplitude and phase synchronization must be made to guarantee the system stability and the continuity of the power system operation. Besides the AC coupling, DC coupling is also a promising alternative, where DC level equalization is an important issue instead of the frequency, amplitude and phase synchronization as in the AC coupling.

Figure 1 presents a photovoltaic system and AC power electric, which are integrated with DC power line coupling and connected to AC and DC loads. The DC line is provided due to the fact that most of electronic appliances require DC power sources, for example, desktop computers, laptop, printers, gadgets, TV, LED lamps, and home audio systems. Even, air conditioners and refrigerators can be driven by DC motors that require DC power source.

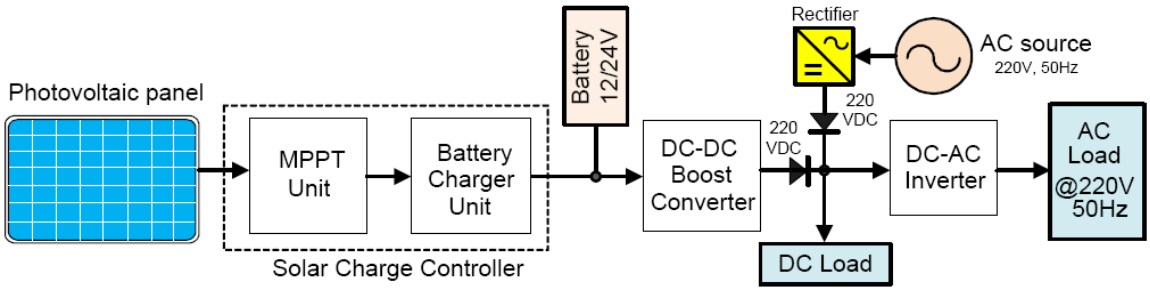

FIGURE 1. A photovoltaic system with DC coupling or DC integration of DC and AC electric power source

The power is integrated in DC 220V. The AC voltage from the grid is rectified to integrate it with the DC voltage from the PV system. The maximum power point tracing (MPPT) unit presented in the figure is used to operate the PV system at its maximum power point [1]. The PV and MPPT modules produce electric power with variant DC voltage. Therefore, a DC-DC boost converter is used as voltage regulator to maintain the voltage level at the expected DC 220V.

This paper discusses mainly on the DC-DC boost converter, and particularly introduces a semi adaptive control, which regulates the step-up process of a varying input voltage from the MPPT unit onto a stable DC output voltage. The contribution presented in this paper is the simplicity to implement the semi adaptive control by tuning the PI controller parameters with simple interpolation equations and look-up table concept. A fully adaptive control can potentially be trapped at divergence situations due to noise or parameter uncertainty. The simplicity of our semi adaptive control contributes to low power consumption of the control algorithm, and can avoid the control algorithm from unstable condition.

In order to present the idea clearly, this paper is organized as follows. Section 2 discusses briefly some works related to this paper. Section 3 describes the concept and formal model to implement the proposed control algorithms. Section 4 shows performance comparisons between the proposed and existing control algorithms through simulations. Section 5 gives a brief discussion of gain adaptation case studies. Finally, Section 6 concludes the work.

2. **Related Works.** There are some circuit topologies that can be used to implement a switched mode voltage regulator, among which are SEPIC [2], Cuk, Switched Capacitor [3], and Charge Pump [4, 5]. Charge Pump is an interesting topology due to the absence of inductor to implement the converter. Unfortunately, because of that, it is difficult to achieve higher voltage gain. By inserting a booster circuit having one or more inductor elements at the input side of the charge pump (CP) circuit, higher voltage gain can be achieved. We adopt the circuit topology from [6] that combines the CP and the booster circuit. However, the circuit presented in that work is designed without a closed loop control. When the input voltage varies and load value changes, the circuit without a closed loop control cannot maintain the output voltage at a certain expected DC level.

As shown in Table 1, most of the DC-DC converters are not equipped with a closed loop control. Voltage regulator with a fully adaptive controller [7] is, in any case, effective to control the output voltage. Nevertheless, fully adaptive control algorithm can be trapped at any unstable points or be divergent, especially at noisy environments. Hence, model-free control method is a challenging alternative [8]. We give a specific contribution in our

Table 1. Comparison of DC-DC converters with high voltage gain

Ref., year	Converter type	Voltage gain	With closed-loop control?
[12], 2014	Two CP capacitors	73V output from 25V input	no
[13], 2014	Switched capacitor-based active network	200V output from 20-40V input	no
[9], 2014	Integrated coupled-inductor and diode-capacitor	380V output from 18-36V input	yes, DSP-based closed-loop control
[10], 2014	Isolated bidirectional converter with winding-cross-coupled inductors	42-56V output from 48-800V input	yes, phase shift control
[11], 2016	Soft-Switching Non-Isolated with Integrated Interleaved Buck-Boost	380V output from 40-60V input	yes, PI control with some logic operations (phase-shifting)
[14], 2016	Two interleave boost stage with 4 stage CP	400V output from 20V input	no
[15], 2015	Voltage Multiplier	380V output from 40V input	no
[16], 2015	Nonisolated, adopting switched capacitor cell	380V output from 25-45V	no
[17], 2016	2nd order hybrid boost	380V output from 35V input	no
[6], 2017	Interleaved input voltage with modified Dickson CP	400V output from 20V input	no
This paper, 2018	Interleaved input voltage with modified Dickson CP	220V output from 12-24V input	yes, interpolated and LUT PI gain scheduling

paper by completing the boosted-input CP circuit with a simple semi adaptive PI control algorithms, which can be classified as model-free control scheme.

The proposed control methods can maintain the output DC voltage level constant at 220V, although the input voltage and load are changed in the simulation. The works in [9, 10] have presented a closed loop control for a DC-DC converter. However, experimental tests with input voltage and load changes have not been verified by the works. Compared to the work in [11] that uses dual duty ratio control signals to shift the phases of its two PWM signals, we propose only a single duty-ratio control signal to control a single uniform PWM signal. Hence, our work proposes a simpler mechanism to regulate the output voltage level.

3. The Concept and Formal Model of the Control Methods.

3.1. The system diagram.

The system diagram of the DC-DC converter with voltage controller is presented in Figure 2(a). In the figure, we can also see the PWM signal waveform (PWM1 and PWM2 signals) showing three modes of operations. The DC-DC converter is built from an interleaved booster, at the input side, and a Dickson Charge Pump topology, at the output side. The NMOS pair (M_1 and M_2) is used to switch the charge pumping configuration.

The PWM signal generations for the transistor switches are presented in Figure 2(b). The PWM signal generation for M_2 is delayed about half-period of the PWM signal generation for M_1. The PWM signal V_{PWM} is obtained by comparing the saw-tooth signal (V_{SAW}) with the control signal (V_{CTRL}). The V_{CTRL} signal is generated by the PI controller. When $V_{CTRL} > V_{SAW}$, then V_{PWM} is in HIGH logic. When $V_{CTRL} \leq V_{SAW}$, then V_{PWM} is in LOW logic. The level of the V_{CTRL} is bounded between V_{LIMIT} at the bottom limit and the maximum value of the V_{SAW} at the top limit.

Due to the signal boundary, the DC-DC converter operates in three modes, as explained in the following.

- **Mode 1** – M_1 and M_2 are ON. When both PWM1 and PWM2 are in logic HIGH, then the NMOS M_1 and M_2 conduct currents (in ON state). In this case, the currents (electric charges) from the voltage source V_{in} are stored in the inductors L_1 and L_2.
- **Mode 2** – M_1 is ON and M_2 is OFF. When PWM1 is on logic HIGH and PWM2 is in logic LOW, then the NMOS M_1 conducts currents (in ON state), while the NMOS M_2 is in OFF state. In this case, the currents (electric charges) from the voltage source V_{in} are stored in the inductor L_1, and in parallel, the electric charges stored in L_2 are discharged to flow to the capacitors C_1 and C_3. A number of currents flow to the load connected in the output terminal.
- **Mode 3** – M_1 is OFF and M_2 is ON. When PWM1 is on logic LOW and PWM2 is in logic HIGH, then the NMOS M_2 conducts currents (in ON state), while the NMOS M_1 is in OFF state. In this case, the currents (electric charges) from the voltage source V_{in} are stored in the inductor L_2, and in parallel, the electric charges stored in L_1 are discharged to flow to the capacitors C_2 and C_4. A number of currents flow to the load connected in the output terminal.

The charge pumping process is guided by the sequences of the operation modes mentioned above. The order of the sequences is Mode 1-Mode 2-Mode 1-Mode 3 and is repeated sequentially as given. The charge pumping process can increase or decrease the output voltage level at terminal $V_{7,0}$ in the circuit. The voltage levels are controlled by the duty ratio of the PWM signals.

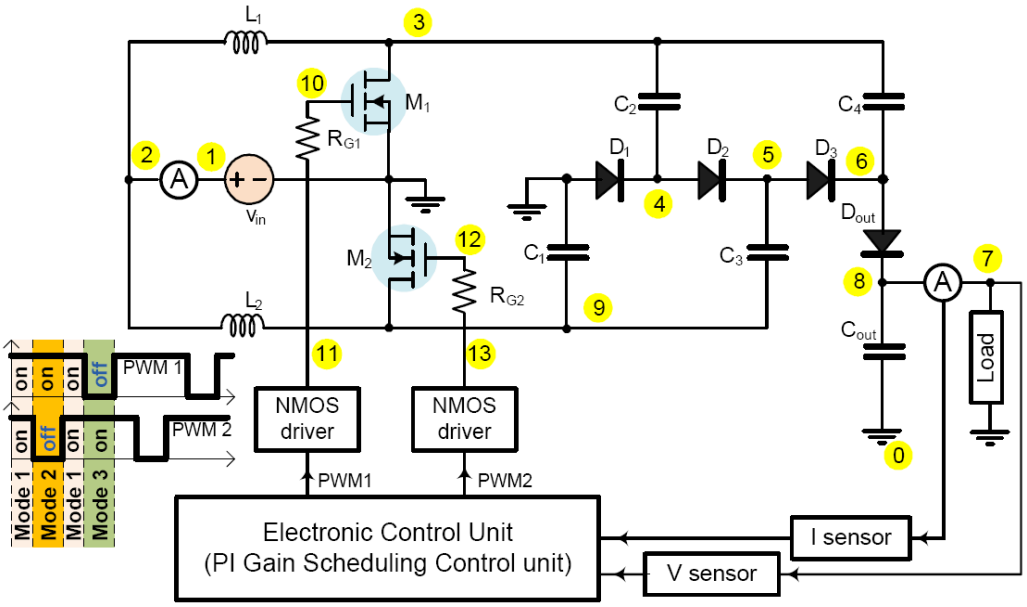

(a) DC-DC converter schematic

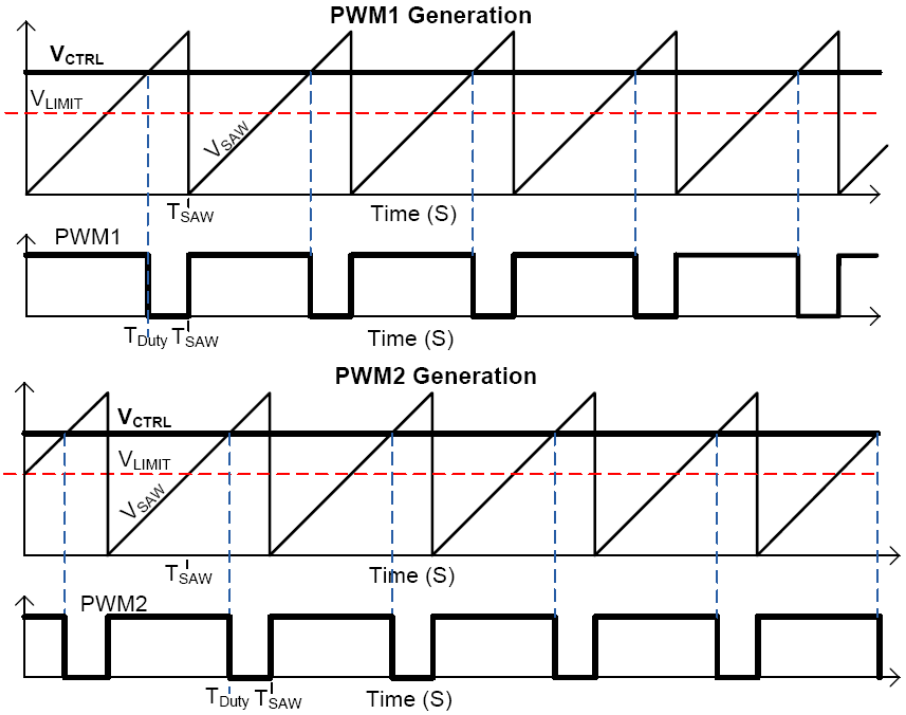

(b) PWM signal generation

FIGURE 2. The DC-DC converter with voltage controller and the PWM signal generation

3.2. **Gain explorations.** Before the interpolation equation or function is derived, and the content of the look-up table is assigned, explorations of the best possible PI gains are made offline or before runtime control process using a simulator tool. In this section, the gain exploration through simulations is presented. Since there is a wide domain of K_P and K_I values that can be explored, only selected values are presented in this work. We select some K_P and K_I values, and then analyze the time domain transient responses of the converter's output voltage. Two criteria or metrics are used to quantify the analysis,

i.e., the average absolute voltage error or AAVE, and the maximum peak (overshoot) or M_P values of the output voltage. The selection process of the relatively best K_P and K_I values for both criteria is described as follows.

- In the M_P criteria, the best PI parameter points (K_P and K_I), which have peak value nearest from the expected 220 V, are selected for each input voltage and load value.
- In the AAVE criteria, the best PI parameter points (K_P and K_I), which have the lowest AAVE value, are selected for each input voltage and load value.

PI gain exploration results for maximum peak (M_P) criteria with 12V DC and 24V DC input voltage and variable resistance load values, i.e., (a) 100Ω, (b) 300Ω, (c) 500Ω and (d) 1000Ω are presented in Figure 3. From the figure, we can see that higher K_P values tend to give higher maximum peak values. Therefore, the smaller K_P values become relatively the best values. Meanwhile, the best K_I depends on the load condition, or the best K_I value is not the same for every different load setting.

PI gain exploration results for average absolute voltage value error (AAVE) criteria with 12V DC and 24V DC input voltage and variable resistance load values, i.e., (a) 100Ω, (b) 300Ω, (c) 500Ω and (d) 1000Ω are presented in Figure 4. As shown in the figure, relative larger or middle range K_P values tend to give lower AAVE. It means that for almost all load cases, the larger K_P values or the middle range values become relatively the best values. Meanwhile, like the previous simulation, the best K_I depends on the load condition.

Based on the PI parameters explorations, we can then select the relatively best selected PI parameters for each criterion, input voltage and load conditions. Figure 5 presents also the relative best PI parameters for different criteria, load and input voltage conditions. It seems that the relatively best K_P and K_I plots present a non linear characteristic. For different load conditions and input voltages, the best PI parameters are not the same. The only one unique characteristic is presented by the best K_P for 12V input voltage with the AAVE criteria, which presents a linear curve. Because of the non linear characteristic, the best PI control parameters should be scheduled based on the selected load condition and criteria.

3.3. **The gain control scheduling.**

3.3.1. *Static PI controller.* In the static PI controller, two static PI gains are selected to simulate, i.e., static PI 1 and static PI 2. In the static PI 1, we select a single pair K_P and K_I gain based on the AAVE criteria, while in the static PI 2, we select a single pair K_P and K_I gain based on the M_P criteria.

3.3.2. *Adaptive interpolated PI gain scheduling controller.* In this control method, the K_P and K_I gain of the PI controller is obtained from interpolation equations. Since there are two input voltage points used in the gain exploration, then for each load condition, the proportional gain is firstly selected based on the equation $K_P = 0.5\left(K_P^{*AAVE} + K_P^{*Mp}\right)$, where K_P^{*AAVE} is the relatively best K_P for the AAVE criteria, and K_P^{*Mp} is the relatively best K_P for the M_P criteria. Meanwhile, the integral gain is firstly selected based on equation $K_I = 0.5\left(K_I^{*AAVE} + K_I^{*Mp}\right)$, where K_I^{*AAVE} and K_I^{*Mp} are the relatively best K_I for the AAVE criteria and the M_P criteria, respectively.

We have made gain explorations for two input voltage points. There are many possible input voltage levels. However, only two input voltage levels are selected, i.e., 12V and 24V. These two points are then used to generate a linear interpolation equation as a function of ΔV as the independent variable, where $\Delta V = V_{REF} - V_{in}(t)$. More input

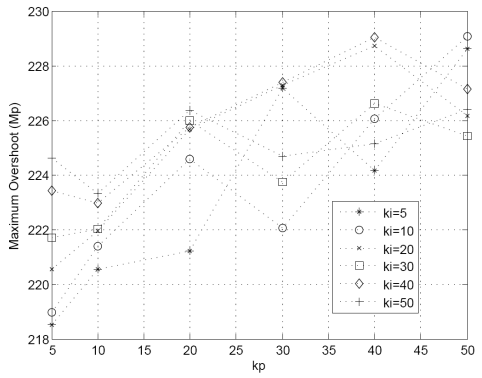

(a) Load 100Ω, $V_{in} = 12$V

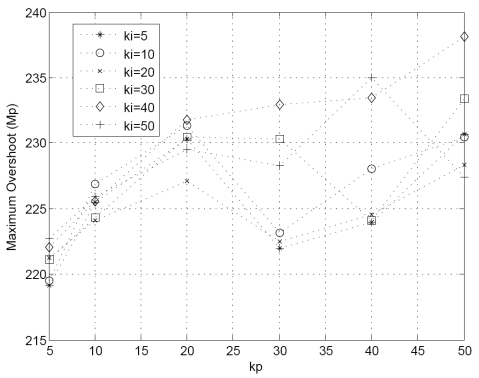

(b) Load 100Ω, $V_{in} = 24$V

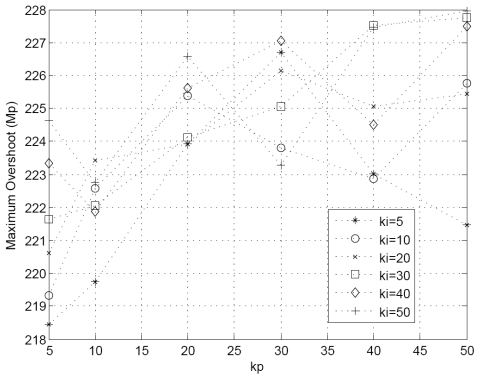

(c) Load 300Ω, $V_{in} = 12$V

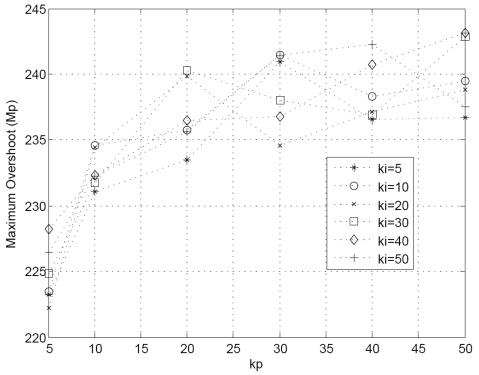

(d) Load 300Ω, $V_{in} = 24$V

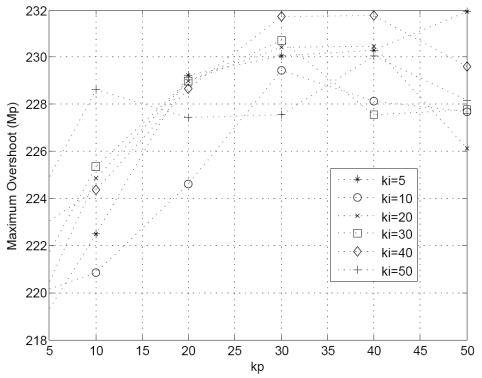

(e) Load 500Ω, $V_{in} = 12$V

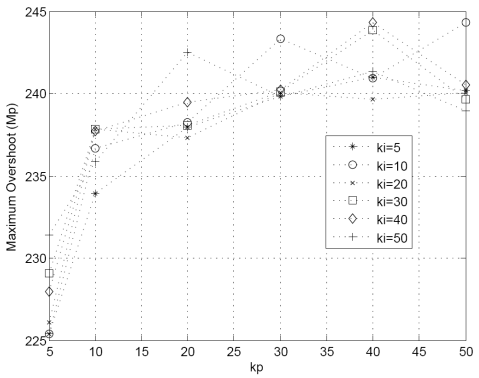

(f) Load 500Ω, $V_{in} = 24$V

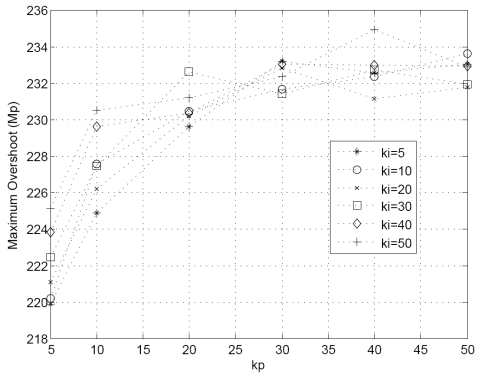

(g) Load 1kΩ, $V_{in} = 12$V

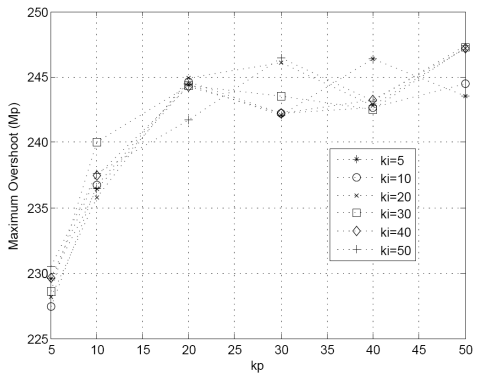

(h) Load 1kΩ, $V_{in} = 24$V

FIGURE 3. PI gain explorations for maximum peak voltage M_P criteria

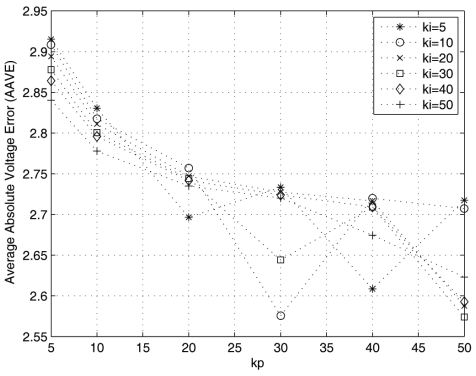

(a) Load 100Ω, V_{in} = 12V

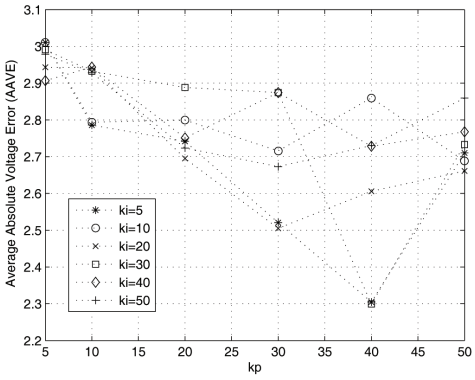

(b) Load 100Ω, V_{in} = 24V

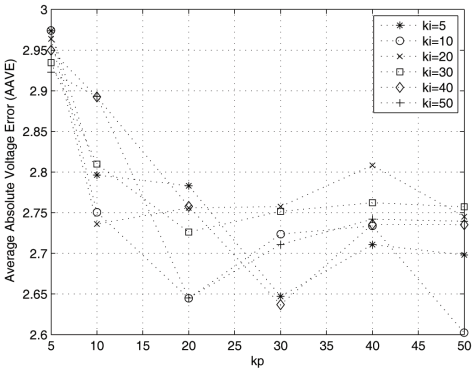

(c) Load 300Ω, V_{in} = 12V

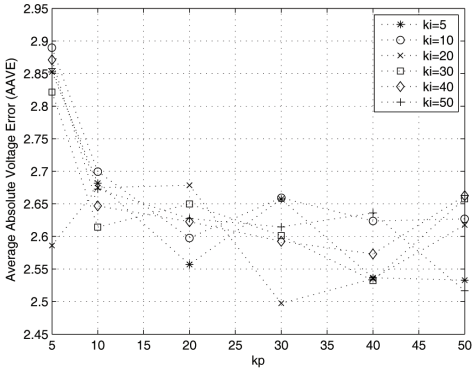

(d) Load 300Ω, V_{in} = 24V

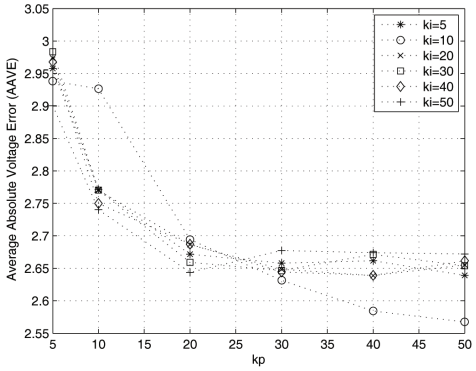

(e) Load 500Ω, V_{in} = 12V

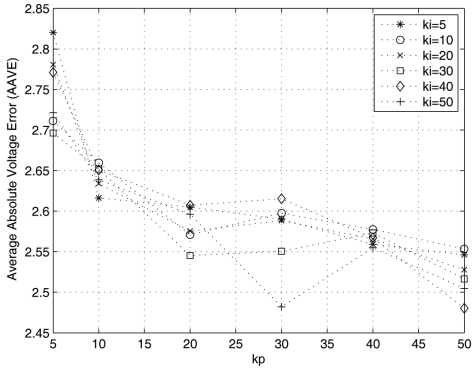

(f) Load 500Ω, V_{in} = 24V

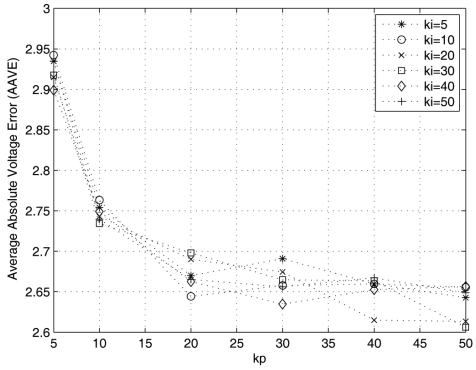

(g) Load 1kΩ, V_{in} = 12V

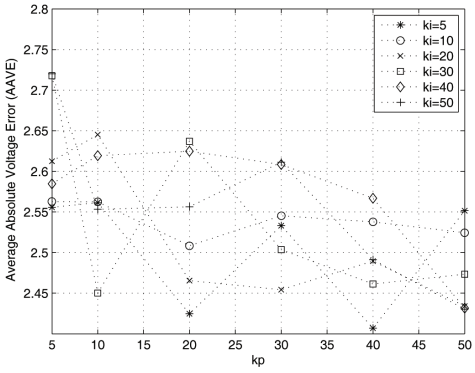

(h) Load 1kΩ, V_{in} = 24V

FIGURE 4. PI gain explorations for average absolute voltage value error (AAVE) criteria

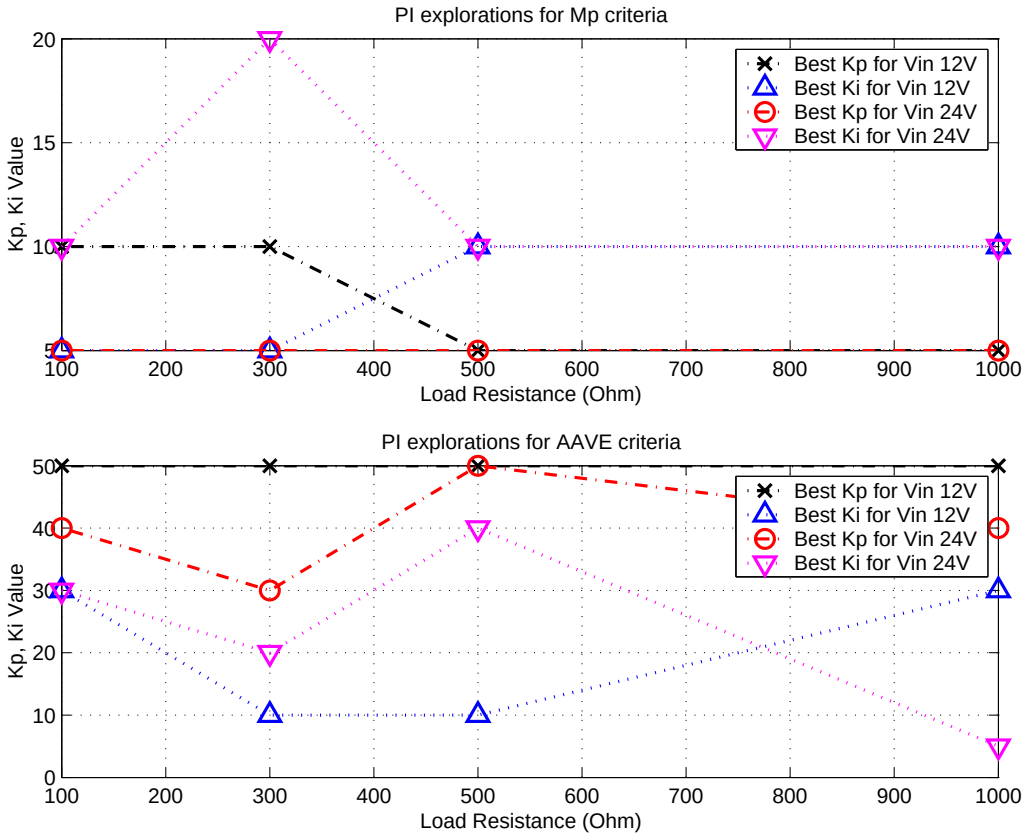

FIGURE 5. The relative best PI parameters for different criteria, load and input voltage conditions

voltage points can be chosen, but it will result in more complex higher order interpolation equation. The achieved interpolation equations of the K_P^* and K_I^* for each load domain are presented in Equation (1) and Equation (2), respectively. The PI gains are selected depending on four different load conditions.

$$K_P^* = \begin{cases} -0.625\Delta V - 100, & 0 \leq Z_{Load} < 100\Omega \\ -1.0417\Delta V - 186.47, & 100 \leq Z_{Load} < 300\Omega \\ 27.5, & 300 \leq Z_{Load} < 500\Omega \\ -0.4167\Delta V - 59.167, & Z_{Load} \geq 500\Omega \end{cases} \tag{1}$$

$$K_I^* = \begin{cases} 0.2083\Delta V + 60.833, & 0 \leq Z_{Load} < 100\Omega \\ 1.0417\Delta V + 224.17, & 100 \leq Z_{Load} < 300\Omega \\ -1.25\Delta V + 270, & 300 \leq Z_{Load} < 500\Omega \\ -1.041\Delta V - 196.67, & Z_{Load} \geq 500\Omega \end{cases} \tag{2}$$

3.3.3. *Adaptive look-up table PI gain scheduling controller.* In this control scheme, the K_P and K_I are selected based on two time domains, i.e., the transient time and steady-state time domain operations. The controller PI gains, ($K_{Pj}^*(k)$ and $K_{Ij}^*(k)$), $j \in [1, 2, 3, 4]$ as presented in Equation (3) and Equation (4), are the function of the gain at any transient time k. The k term is the index number in the look-up table. The K_P^* and K_I^* selections

are made based on these two time domains.

$$K_P^* = \begin{cases} K_{P1}^*(k), & 0 \leq Z_{Load} < 100\Omega \\ K_{P2}^*(k), & 100 \leq Z_{Load} < 300\Omega \\ K_{P3}^*(k), & 300 \leq Z_{Load} < 500\Omega \\ K_{P4}^*(k), & Z_{Load} \geq 500\Omega \end{cases} \tag{3}$$

$$K_I^* = \begin{cases} K_{I1}^*(k), & 0 \leq Z_{Load} < 100\Omega \\ K_{I2}^*(k), & 100 \leq Z_{Load} < 300\Omega \\ K_{I3}^*(k), & 300 \leq Z_{Load} < 500\Omega \\ K_{I4}^*(k), & Z_{Load} \geq 500\Omega \end{cases} \tag{4}$$

As presented in Equation (5), the time domains are bounded by the boundary-state voltage value V_{BS}. The value of the V_{BS} can be determined carefully to be a constant voltage value such as 5V or 7V above and below the steady-state voltage (V_{SS}) or reference voltage V_{REF}. In our case, the value of the V_{REF} is 220V. The V_{BS} value is set to 5V/7V, because when the output voltage V_{Load} is within the range of $V_{SS} \pm 5V$ or $V_{SS} \pm 7V$, then the selection of the PI control parameters is changed from transient to steady state criteria. If the absolute error voltage $V_E(t) = V_{REF} - V_{Load}(t)$ is greater than or equal to V_{BS}, then the best K_P and K_I values ($k_{transient}^*$) from the look-up table for the maximum peak overshoot criteria will be used. Else, if the $V_E(t)$ is less than V_{BS}, then the best K_P and K_I values (k_{steady}^*) from the look-up table for the AAVE criteria will be used.

$$k = \begin{cases} k_{transient}^*, & |V_E(t)| \geq V_{BS} \\ k_{steady}^*, & |V_E(t)| < V_{BS} \end{cases} \tag{5}$$

4. **The Performance Comparison.** In this section, the performances of four control methods are compared through simulation, i.e., the static PI 1, static PI 2, the adaptive interpolated PI gain scheduling and the adaptive look-up table PI gain scheduling control method. Two scenarios are used for the performance test with dynamically changed input voltage, i.e., as presented in Figure 6(a) and Figure 6(b). From both figures, it seems that the transient characteristics of the adaptive interpolated and adaptive LUT PI GS control methods are better than the static PI control methods.

Table 2 presents the summarized performance comparisons of the control methods simulated before. As shown in the table, we can see that the adaptive look-up table (LUT) PI gain scheduling control method presents the best performance over the other control methods. Measured relative to the expected 220V, its average absolute output voltage error is below 1.141% with maximum overshoot about 5.6%.

5. **Brief Discussion of Gain Adaptation Case Studies.** In some voltage regulator or power supply application cases, PI or PID controller gains should be adapted to follow load changes and input voltage variation [18]. This action is made in order to meet a single or multiple objectives such as maintaining rated output voltage or improving power efficiency or output power. PV-based power systems as a particular case shows the phenomena. When power demand represented by an electric load is lower than the generated power, the output voltage will be higher than the rated voltage [19]. Another case is also presented in a synchrotron beam source application [20], where the discrete PID gain should be adapted for magnetic load change in order to meet control objective.

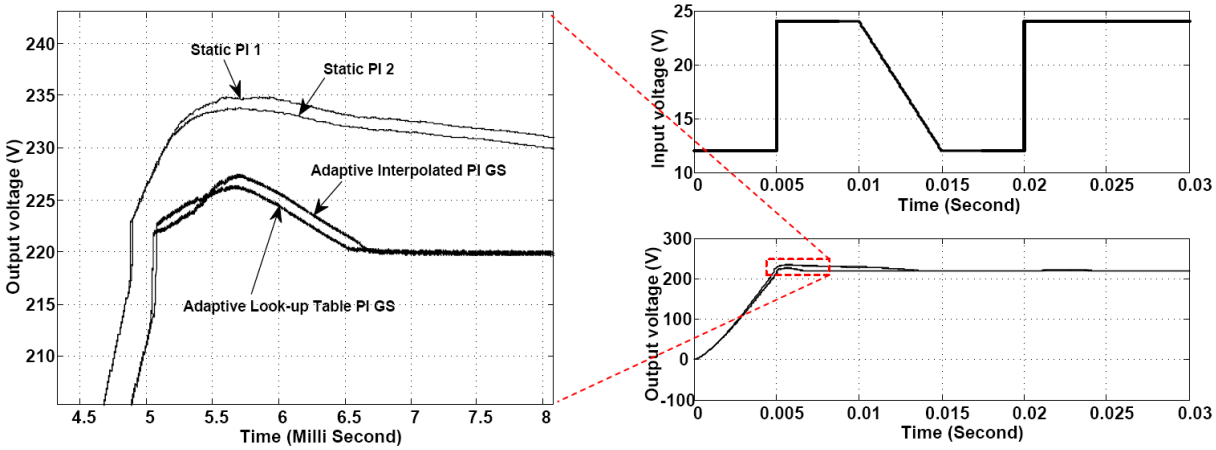

(a) Test Case 1

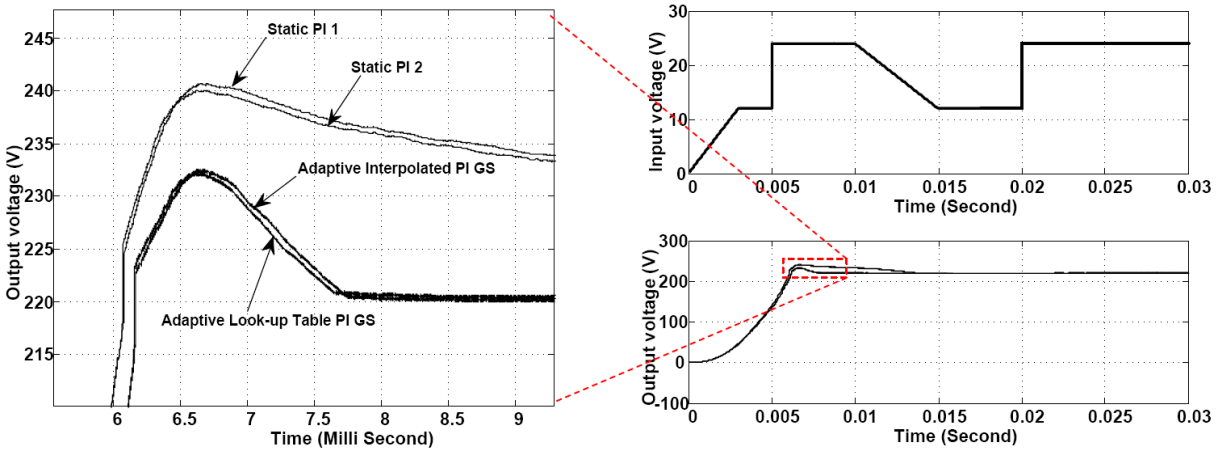

(b) Test Case 2

FIGURE 6. Test scenario with variable input voltages

TABLE 2. Performance comparison of the control methods

Control method	Max. Peak	AAVE	Settling time
Static PI 1	241.612V	3.1989V	10.938ms
Static PI 2	240.725V	3.1077V	10.927ms
Adapt. Interp. PI GS	232.564V	3.0992V	6.875ms
Adaptive LUT PI GS	232.338V	3.0990V	6.823ms

6. **Conclusions.** This paper has presented an adaptive interpolated PI gain scheduling and adaptive look-up table (LUT) PI gain scheduling (GS), which effectively reduce the maximum overshoot of the DC-DC converter output voltage during transient conditions. In average, both methods can decrease the maximum overshoot between 5.6% and 5.71%, which are saved enough for real implementation in PV-based electric power systems. The adaptive LUT PI GS outperforms slightly its counterpart adaptive interpolated PI GS. The performance differences are not significant, when it is compared to the static PI control. The adaptive LUT PI GS gives about 8V better maximum peak overshoot, about 0.1V better AAVE and about 4 seconds faster settling time compared to the static PI control method.

The performance improvements of the adaptive LUT PI GS control method are not so significant compared to the performance of the adaptive interpolated PI GS control method, i.e., only about 0.0013% lower maximum peak overshoot, 0.000065% smaller AAVE and 0.0076% faster settling time. However, the control algorithm of the adaptive LUT PI GS control method is more simple. It is even much more simple compared to fully adaptive control algorithms. The adaptive LUT PI GS control algorithm is implemented with a simple look-up table gain selection based on the transient and steady-state time domain operations.

Certainly, there are many possible approaches that can be used to construct the interpolated and LUT-based PI gain scheduling control method. This paper presents only a few representations of them, and also at least as a basic guide to construct a simple semi adaptive control that can work effectively to control the output voltage of the DC-DC control at a stable DC operating point. Extension and advancements of our approach to obtain more optimal results are still open.

Acknowledgement. We gratefully acknowledge the Ministry for Research, Technology and Higher Education of the Republic of Indonesia (by *Direktorat Riset dan Pengabdian Masyarakat*, DRPM) for funding and supporting our research work under the scheme of "Post Graduated Colleagium Research Grant" (*Hibah Penelitian Tim Pasca Sarjana*) in the years 2017 and 2018.

REFERENCES

[1] F. A. Samman, A. A. Rahmansyah and Syafaruddin, Peak bracketing and decremented window-size scanning-based MPPT algorithms for photovoltaic systems, *International Journal of Innovative Computing, Information and Control*, vol.14, no.3, pp.1015-1028, 2018.

[2] R. S. Vadivoo, S. Vijayalakshmi and K. Vairamarri, Design of ZVS resonant SEPIC converter for high frequency applications, *Proc. of the 2014 IEEE Int'l Conf. on Circuit, Power and Computing Technologies (ICCPCT)*, pp.873-880, 2014.

[3] W. Do and K. Eguchi, A control way of a Fibonacci sequence switched capacitor DC-DC converter for higher power efficiency, *ICIC Express Letters*, vol.12, no.1, pp.55-60, 2018.

[4] J. Dickson, On-chip high-voltage generation MNOS integrated circuits using an improved voltage multiplier technique, *IEEE J. Solid State Circuits*, vol.11, no.3, pp.374-378, 1976.

[5] G. Palumbo and D. Papalardo, Charge pump circuits: An overview on design strategies and topologies, *IEEE Circuit and Systems Magazine*, vol.10, pp.31-45, 2010.

[6] B. P. Baddipadiga and M. Ferdowsi, A high-voltage-gain DC-DC converter based on modified Dickson charge pump voltage multiplier, *IEEE Trans. Power Electronics*, vol.32, no.10, pp.4206-4216, 2017.

[7] R. Madhumitha and R. Vinothkumar, Voltage regulation in mircogrid using adaptive controller, *Proc. of the 2014 Int'l Conf. on Green Computing Communication and Electrical Engineering (ICGCCEE)*, pp.1-5, 2014.

[8] L. He and K. Li, Simulation study on model-free control method in DC-DC converter, *Proc. of the 8th 2016 IEEE Int'l Conf. on Intelligent Human-Machine Systems and Cybernetics (IHMSC)*, pp.60-63, 2016.

[9] X. Hu and C. Gong, A high voltage gain DC-DC converter integrating coupled-inductor and diode-capacitor techniques, *IEEE Trans. Power Electronics*, vol.29, no.2, pp.789-800, 2014.

[10] W. Li, C. Xu, H. Yu, Y. Gu and X. He, Analysis, design and implementation of isolated bidirectional converter with winding-cross-coupled inductors for high step-up and high step-down conversion system, *IET Power Electronics*, vol.7, no.1, pp.67-77, 2014.

[11] H. Wu, T. Mu, H. Ge and Y. Xing, Full-range soft-switching isolated buck-boost converters with integrated interleaved boost converter and phase-shifted control, *IEEE Trans. Power Electronics*, vol.31, no.2, pp.987-999, 2016.

[12] M. R. A. Siddique, M. J. Ferdous and I. Islam, Charge pump capacitor based high voltage gain DC-DC step-up converter, *Proc. of the 2014 IEEE Int'l Conf. on Informatics, Electronics & Vision (ICIEV)*, pp.1-4, 2014.

[13] Y. Tang, T. Wang and Y. He, A switched-capacitor-based active-network converter with high voltage gain, *IEEE Trans. Power Electronics*, vol.29, no.6, pp.2959-2968, 2014.

[14] V. A. K. Prabhala, P. Fajri, V. S. P. Gouribhatla, B. P. Baddipadiga and M. Ferdowsi, A DC-DC converter with high voltage gain and two input boost stages, *IEEE Trans. Power Electronics*, vol.31, no.6, pp.4206-4216, 2016.

[15] K.-C. Tseng, C.-C. Huang and C.-A. Cheng, A high step-up converter with voltage-multiplier modules for sustainable energy applications, *IEEE Journal of Emerging and Selected Topics in Power Electronics*, vol.3, no.4, pp.1100-1108, 2015.

[16] G. Wu, X. Ruan and Z. Ye, Nonisolated high step-up DC-DC converters adopting switched-capacitor cell, *IEEE Trans. Industrial Electronics*, vol.62, no.1, pp.383-393, 2015.

[17] B. Wu, S. Li, Y. Liu and K. M. Smedley, A new hybrid boosting converter for renewable energy applications, *IEEE Trans. Power Electronics*, vol.31, no.2, pp.1203-1215, 2016.

[18] C.-S. Shieh, An FPGA-based sliding fuzzy control for DC/DC boost converter, *ICIC Express Letters*, vol.12, no.2, pp.167-174, 2018.

[19] M.-T. Tsai, C.-L. Chu, Y.-J. Yang and D.-J. Wu, Design of a dual active bridge DC-DC converter for photovoltaic system application, *ICIC Express Letters, Part B: Applications*, vol.7, no.8, pp.1805-1812, 2016.

[20] Y. Chien, C. Liu and B. Wang, A digital fast corrector power converter sesign for TPS ring, *ICIC Express Letters, Part B: Applications*, vol.8, no.7, pp.1085-1093, 2017.